Food Chemistry 508 (2026) 148452

Contents lists available at ScienceDirect

Food Chemistry

journal homepage: www.elsevier.com/locate/foodchem

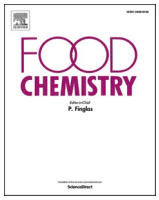

Optimal integration of lignin nanoparticles and whey protein distinctively stabilizes high internal phase pickering emulsions for multiple environmental resistances

Guilan Zhao [a], Qian Zhang [a], Yongtai Wang [a,b], Xiaojie Gao [a], Fei Huang [a], Jiale Liu [a], Hao Peng [a,c], Chunxiang Fu [c], Yanting Wang [a,*], Liangcai Peng [a,b,*]

[a] Key Laboratory of Fermentation Engineering (Ministry of Education), National "111" Center for Cellular Regulation & Molecular Pharmaceutics, Cooperative Innovation Center of Industrial Fermentation (Ministry of Education & Hubei Province), Hubei Key Laboratory of Industrial Microbiology, Biomass & Bioenergy Research Center, School of Life & Health Sciences, Hubei University of Technology, Wuhan 430068, China
[b] College of Plant Science & Technology, Huazhong Agricultural University, Wuhan 430070, China
[c] Shandong Provincial Key Laboratory of Energy Genetics, CAS Key Laboratory of Biofuels, Qingdao Institute of Bioenergy & Bioprocess Technology, Chinese Academy of Sciences; Shandong Energy Institute; Qingdao New Energy Shandong Laboratory, Qingdao 266101, China

ARTICLE INFO

Keywords:
Pickering emulsions
Lignin nanoparticles
Whey protein
Emulsion stability
Rheological properties
Curcumin encapsulation, bioparticles interaction

ABSTRACT

High internal phase Pickering emulsions (HIPPEs) are increasingly explored for sustainable food industries, but they rely on advanced solid particles stabilizers. In this study, we constructed an optimal lignin nanoparticles-whey protein (LNPs-WP) complex system to stabilize Pickering emulsions by forming a viscoelastic membrane at the oil-water interface through electrostatic attraction. The HIPPEs stabilized by LNPs-WP at high ratios (6:8–8:8) exhibited smaller oil droplets ($d_{4,3}$ < 20 μm), higher viscosity, stronger elastic moduli and better thixotropic recovery. Notably, the optimal LNPs-WP (8:8) nanocomplexes maintained the emulsions with exceptional storage stability for 90 days, high thermal resistance up to 90 °C and strong ionic resistance with 1000 mM NaCl. Furthermore, the HIPPEs with the optimal LNPs-WP enabled 78% curcumin retention after 96 h UV-irradiation. Therefore, this study has demonstrated a powerful and green strategy for evolving desirable Pickering emulsions stabilization by optimal integration of natural bioparticles, providing a broad application in functional foods, pharmaceuticals, cosmetics and beyond.

1. Introduction

Pickering emulsions as stabilized by solid particles instead of traditional surfactants, have gained a significant attention from their unique advantages. Unlike surfactant-stabilized emulsions, Pickering emulsions exhibit superior stability against coalescence, Ostwald ripening, and environmental changes (e.g., temperature, pH, and ionic strength) (Jiang, Sheng, & Ngai, 2020; Zhao et al., 2025). As the solid particles form a dense and irreversible barrier at oil-water interface, they reduce the risk of emulsions breakdown during processing and storage to effectively encapsulate sensitive bioactive compounds such as curcumin, vitamins, and phenolic compounds. Therefore, environmentally-friendly biopolymer particles are increasingly explored for emulsions stabilization (Calabrese, Courtenay, Edler, & Scott, 2018).

Because natural solid biopolymers are biocompatible and biodegradable (Burgos-Díaz et al., 2023; Naji-Tabasi, Mahdian, Arianfar, & Naji-Tabasi, 2021; Peng et al., 2022; Wang et al., 2024), they are increasingly being considered for stabilizing Pickering emulsions, particularly for preparing high internal phase Pickering emulsions (HIPPEs) (Zhao, Wang, Li, Yang, & Song, 2023). HIPPEs are defined as the system with the volume fraction of dispersed phase exceeding 74% to maximize encapsulation efficiency (Kim et al., 2017). Due to a high oil phase concentration and complex internal structure, HIPPEs are of a unique rheological property (Chen et al., 2021), thereby leading to extremely broad applications in food processing (Li, Fan, & Li, 2023), porous material templates (Mikkonen, 2020), and pharmaceuticals

* Corresponding authors at: Key Laboratory of Fermentation Engineering (Ministry of Education), National "111" Center for Cellular Regulation & Molecular Pharmaceutics, Cooperative Innovation Center of Industrial Fermentation (Ministry of Education & Hubei Province), Hubei Key Laboratory of Industrial Microbiology, Biomass & Bioenergy Research Center, School of Life & Health Sciences, Hubei University of Technology, Wuhan 430068, China.
E-mail addresses: wyt@mail.hzau.edu.cn (Y. Wang), lpeng@mail.hzau.edu.cn (L. Peng).

https://doi.org/10.1016/j.foodchem.2026.148452
Received 22 October 2025; Received in revised form 16 January 2026; Accepted 12 February 2026
Available online 15 February 2026

(Moreno & Sipponen, 2020; Zhou et al., 2023).

Among the natural biopolymers, whey protein (WP) has been employed as an active emulsifier due to its excellent surface activity, nutritional value and biocompatibility (Davtalab et al., 2024). Particularly, WP can adsorb at oil-water interface, reduce interfacial tension, and stabilize emulsions through steric hindrance and electrostatic repulsion (Zhu, 2024). However, WP-stabilized emulsions are sensitive to environmental factors such as high temperature and high salt ion concentration, thereby causing emulsion flocculation or coalescence (Chevallier et al., 2016). Moreover, the individual WP often fails to form stable HIPPEs with oil fractions exceeding 74%, restricting its application in high-viscosity products. Alternatively, whey protein modifications are considered to improve emulsifying properties through augmenting thickness of the adsorbed layer, diminishing interfacial tension, achieving equilibrium between repulsive and attractive forces, and boosting viscoelasticity of the interfacial layers (Li, Guo, Dong, & Yang, 2023; Shomali & Fatehi, 2022; Wan et al., 2024). A significant concern is the safety of modified whey proteins including glycated whey protein isolates and associated products (Hellwig et al., 2019). Some physical modifications such as enzymatical modification and ultrasound treatment are rarely used in practical applications due to a high cost (Sarabandi et al., 2022). To tackle the issues of safety and high cost, we herein reported a strategy to synergistically stabilize HIPPEs.

As the second most polymer of plant cell walls, lignin possesses an aromatic composition with a three-dimensional spatial structure composed of syringyl (S), guaiacyl (G), and *p*-hydroxyphenyl (H) units linked by both ether and carbon-carbon bonds (Bai et al., 2019; Yu et al., 2025; Zhang et al., 2020). Due to its complicated structure and diverse functions, lignin has emerged as a desired candidate for stabilizing emulsions (Gan et al., 2025). Importantly, the lignin nanoparticles (LNPs) prepared by downsizing lignin into nanoscale particles are of controllable particle sizes and uniform structures. The LNPs amphiphilic nature is attributed to the hydrophilic hydroxyl groups and hydrophobic aromatic rings, which enables them to effectively adsorb at the oil-water interface and balance wettability for emulsions stabilization (Mikkonen, 2020). Furthermore, LNPs are of antioxidant and UV-shielding properties to protect encapsulated bioactive compounds from oxidative degradation and photolysis (Zhang, Yue, Hu, Qi, & Lu, 2023). Although protein combination with bioparticles is an effective strategy to overcome limitation of single-component emulsifiers, little is yet reported about synergistic impact of WP and LNPs integration. Notably, LNPs possess inherent hydrophobicity and mechanical rigidity-properties that perfectly complement the hydrophilicity and nutritional value of WP while addressing its sensitivity to heat and salt. Thus, we proposed a synergistic stabilization strategy to construct a multifunctional interfacial layer via a combination of hydrophilic whey protein and hydrophobic lignin nanoparticles.

In this study, we aimed to develop Pickering emulsions stabilized by integration of LNPs and WP, and evaluated their microstructure, rheological properties, and stabilization capacity. We also detected the dynamic changes of emulsion stability under different conditions of internal phase fraction, storage time and temperature, and salt ion concentration. Furthermore, this study assessed the capacity of encapsulating curcumin as a bioactive compound with poor water solubility and photostability, and expanded its applications in functional food and nutraceuticals. Finally, a model was proposed to highlight the Pickering emulsions improvements at five distinct properties (ultra-high internal phase, storage stability, thermal stability, ionic stability, curcumin remain under UV), thereby providing insights into designing the sustainable Pickering emulsions with high performances via natural biopolymers and nanoparticles.

2. Materials and methods

2.1. Materials and chemicals

Alkali lignin after the dealkalization was obtained from Macklin Chemical Reagent Co., Ltd. (Shanghai, China). Whey protein and soybean oil were purchased from Shanghai Yuanye Biotechnology Co., Ltd. (Shanghai, China) and Jinlongyu Grain and Oil Industry Group Co., Ltd. (Shanghai, China), respectively. Acetone and other reagents were obtained from China National Pharmaceutical Group Chemical Reagent Co., Ltd. (Shanghai, China). All other chemicals are analytical grades.

2.2. Formulation of LNPs and WP interaction systems

LNPs dispersions were prepared via an anti-solvent method as described by Moreno and Sipponen (2020) with minor modifications. The lignin was dissolved in acetone/water solution (3:1, w/w) and insoluble impurities were removed by filtration. Specifically, the LNPs were produced by rapid pouring of deionized water to lignin acetone solution followed by rotary evaporation of acetone, and the final aqueous dispersion of LNPs (2 wt%) was obtained after rotary evaporation. The whey protein (WP, $\geq$90% protein content) was commercially purchased and had undergone spray granulation. The WP solutions were obtained by stirring continuously for 2 h, and left in the refrigerator at 4 °C for 12 h to ensure adequate hydration. The LNPs-WP systems were finally developed by dropping LNPs suspensions into the WP solutions with different LNPs concentrations, stirring continuously for 2 h, and adjusting the resulting complex at the pH 6 by 1.0 M HCl solution. In the experiment investigating the ionic resistance of emulsions, dispersion equilibrium was achieved by introducing sodium ions (200, 400, 600, 800, 1000 mM) into the LNPs-WP through balanced dialysis procedures, while avoiding unintended effects.

2.3. Preparation of emulsions

The mixtures were obtained by dispersing soybean oil in the LNPs-WP systems. The volume ratio of oil phase to the total system is 80–90%. The O/W emulsions were prepared by shearing the resulting mixtures at 11000 r/min for 90 s using a high-speed homogenizer (PD500, GREENPRIMA, UK). Sodium azide (0.02%, w/v) was added in the samples to suppress microbial growth.

In the experiment exploring the effect of temperature on the stability of HIPPEs, the emulsions were heated for 20 min at 25 °C, 65 °C, 90 °C, and 121 °C. And the changes in the microstructure and rheological properties of the emulsions were observed.

2.4. Particle size and ζ-potential

The Zetasizer Nano ZS90 (Malvern Instruments Ltd., UK) was used to measure particle size and ζ-potential of LNPs-WP systems at 25 °C. LNPs-WP systems and emulsions were diluted 30 and 100 times before testing, respectively. Diluted samples (0.5 mL) were placed in a measuring container and scanned automatically by the instrument. The refractive indexes of particle solutions and water were 1.45 and 1.33 respectively. Each sample was determined under independent triplicate.

2.5. Ultraviolet spectrum

UV spectrophotometer (T600, Persee, China) was applied to capture the UV–visible absorption spectra of LNPs, WP, and LNPs-WP dispersions according to Zhao et al. (2024). The measurements were performed with the following settings: a wavelength range of 220–600 nm, a scanning speed of 50 nm/min, a slit width of 2 nm, and a cuvette path length of 1.0 cm.

2.6. High-resolution field emission scanning electron microscope (FE-SEM)

The LNPs, WP, and LNPs-WP solutions were freeze-dried under vacuum for 24 h to remove moisture, and maintained at −40 °C under the vacuum pressure kept at 30 Pa. The dried samples were then attached to conductive carbon tape and coated with gold using a sputtering machine to observe SEM (SU8010, Hitachi, Japan) images as described in a previous study (Li et al., 2024).

2.7. Three-phase contact angle

German-manufactured optical contact angle meter (OCA15EC, Dataphysics Instruments GmbH) was employed to determine the oil-water three-phase contact angle (θ_{ow}) of LNPs-WP systems with some modifications based on the method used by (Tao, Zhu, Zhu, Lei, & Zhao, 2024). The lyophilized LNPs-WP powders were pressed into pellets with a diameter of 13 mm and a thickness of 2 mm. The pellets were then placed into a rectangular glass cuvette, which was pre-filled with soybean oil. About 5 μL droplet of deionized water was dispensed onto the surface of each pellet using an automatic syringe. After allowing 30 s for the system to reach equilibrium, a high-speed video camera was used to capture images of the water droplet. The Laplace-Young equation was thereafter applied to calculate the contact angle from the captured images. To ensure data reliability, at least four water droplets were measured per pellet, and three independent pellets were tested for each LNPs-WP sample.

2.8. Optical microscope and size of emulsion

The microstructure of emulsions was observed under an optical microscope (NE300, Ningbo Yongxin Optics co., Ltd., China). A volume of 10 μL of the emulsions was placed on a slide and magnified 10 or 40 times to observe morphology. The droplet size distributions of the emulsions were analyzed using static light scattering at 25 °C coupled with a Malvern MasterSizer 2000 instrument (Malvern Instruments Ltd., Malvern, Worcestershire, U.K.). To ensure accurate measurements, the samples were diluted to achieve an obscuration level between 2% and 4%. The refractive indices were calibrated to 1.46 for soybean oil and 1.33 for aqueous phase. The average droplet sizes of the emulsion were calculated as $d_{4,3}$ (the volume mean diameter, $\frac{\sum n_i d_i^4}{\sum n_i d_i^3}$) and $d_{3,2}$ (surface mean diameter, $\frac{\sum n_i d_i^3}{\sum n_i d_i^2}$), where n_i is the number of droplets with diameter d_i.

2.9. Confocal laser scanning microscopy

The emulsion droplets were examined using confocal laser scanning microscopy (CLSM with LSM 980, Zeiss, Germany). Before staining, the sample was diluted 10 times. The 100 μL diluted sample was stained by adding 1 μL of Nile red solution (1 mg/mL in ethanol) and Nile blue solution (1 mg/mL in ethanol). After mixing thoroughly with a vortex oscillator, 5 μL of the dyed sample was placed on a microscope slide and covered with a glass coverslip. The excitation spectra for Nile red and Nile blue were 488 and 633 nm, respectively.

2.10. Rheological measurement

The rheological properties of emulsions were determined using an A Discovery HR-1 Rheometer (TA Instruments Ltd., USA) equipped with a parallel plate (40 mm in diameter, 1 mm gap) as previously described (Wang et al., 2022). The oscillatory experiments included amplitude sweeps (frequency: 1 Hz, stress: 0.1–100 Pa) and frequency sweeps (stress: 0.5 Pa, frequency: 0.1–10 Hz). Apparent viscosity was measured across a shear rate range of 0.1–100 s^{-1} for all samples. In addition, the structure recovery property was measured by three interval thixotropy test (3ITT) at the shear rates of 0.1 s^{-1} (0–120 s), 100 s^{-1} (120–150 s), and 0.1 s^{-1} (150–270 s).

2.11. Turbiscan stability index of emulsions

The physical stability of emulsions was assessed using a Turbiscan Lab Expert analyzer (Turbiscan Tower, Toulouse, France) as previously described by Zhao et al. (2023). This instrument measured both transmission and backscattering separately. Following various storage durations, 20 mL emulsions were transferred into a test glass tube, and the entire height of the samples was scanned at 25 °C. The light intensity was recorded, and the Turbiscan stability index (TSI) was subsequently calculated by the Turbiscan software according to the following formula:

$$TSI = \sqrt{\frac{\sum_{i=1}^{n}(x_i - x_{BS})^2}{n-1}} \quad (1)$$

here, n represents the number of scans, x_i is the average backscattering for each minute, x_{BS} is the overall average backscattering. Lower TSI values indicate more stable emulsions.

2.12. Characterization of curcumin-loaded HIPPEs

A certain amount of curcumin was weighed and dissolved in ethanol to prepare a standard solution with a concentration of 0.01 mg/mL. After diluting, the solution was subjected to spectral scanning in the range of 350–500 nm using a UV–Vis spectrophotometer. Under light-protected conditions, aliquots of the curcumin standard solution (0.1–0.6 mL) were separately transferred into volumetric flasks, diluted to volume, and the absorbance of each solution was measured at the maximum absorption wavelength of 425 nm. A standard calibration curve for curcumin was constructed based on the measured absorbance values.

Preparation of curcumin emulsions according to a previously reported method (Li, Yang, Wang, Xu, & Li, 2024): Oil phase of curcumin emulsions was obtained by weighing 50 mg of curcumin and dissolving in 50 mL of soybean oil. After the mixture was stirred overnight at room temperature, an oil phase containing supersaturated curcumin was obtained. After centrifugation at 16099*g* for 10 min at 25 °C, undissolved curcumin was removed to collect a saturated curcumin oil phase. The curcumin content of emulsions was determined under UV spectrophotometry, and the final aforementioned curcumin oil phase at 0.185 mg/mL (18.5% extraction efficiency) was applied to prepare the LNPs-WP curcumin emulsion as described in Section 2.3.

UV irradiation stability: The curcumin emulsion was placed in a glass bottle with a diameter of 1 cm and a height of 5 cm for UV treatment. The glass bottle was irradiated for 96 h with a distance of 30 cm from UV lamp (30 W, 365 nm) as previously reported by Li, Yang, et al. (2024). Every 12 h, 250 μL of the curcumin emulsion was loaded into 9750 μL of anhydrous ethanol, vortexed for 3 min, and centrifuged at 16099*g* for 10 min at room temperature. The absorbance of supernatant was measured at 425 nm under a UV spectrophotometer, and the curcumin content was calculated according to the standard curve and the retention rate obtained. The curcumin oil phase was used as a control to evaluate the protective effect of LNPs-WP emulsion on curcumin.

Storage stability: Curcumin was dissolved in oil to prepare emulsion, and the emulsion was placed under sunlight for 21 days, and the change of curcumin content was measured by ultraviolet spectrophotometer with the retention rate calculated.

2.13. Statistical analysis

All experiments were conducted in triplicate independently. The results are presented as mean values ± standard deviation. Statistical

analysis was performed using one-way ANOVA and two-tailed *t*-test with the software SPSS 26 (Chicago, IL) to determine significant differences between means ($*p < 0.05$, $**p < 0.01$).

3. Results and discussion

3.1. Effective integration of lignin nanoparticles with whey protein

In this study, lignin nanoparticles (LNPs) were initially extracted using previously-established method (Moreno & Sipponen, 2020), and then integrated with whey protein (WP) at different mass ratios for construction of LNPs-WP composites as bioparticles (Fig. 1). As a result, the bioparticles exhibited a bimodal distribution pattern, and their sizes were gradually increased while the LNPs concentrations remained raising (Fig. 1A). At high ratios of LNPs-WP (6:8–8:8), the bioparticle sizes showed a unimodal distribution, suggesting that the particles become uniform shapes. Particularly, a narrower particle size distribution was observed from high ratios of LNPs-WP, indicating that the addition of LNPs could cause a better dispersibility of the particles. The results of the polydispersity index (PDI) gradually decreased while the amount of LNPs was increasingly added. Meanwhile, the zeta potential results revealed that LNPs can enhance the electrostatic repulsion of WP (Fig. 1B), which may account for the improved dispersibility of the LNPs-WP particles. It also suggested that LNPs and WP may bind through electrostatic interactions.

Furthermore, this study examined the UV spectra of LNPs-WP bioparticles at varying ratios (Fig. 1C). In general, a characteristic absorption peak of lignin was located at 280 nm, attributing to the $\pi \rightarrow \pi^*$ transition of benzene ring within lignin molecule. In particularly, the LNPs exhibited a pronounced UV absorption peak at 361 nm, being consistent with the absorption characteristics of phenolic hydroxyl in the near-ultraviolet region (350–370 nm) (Qin et al., 2025). The spectrum of WP dispersion showed an absorption peak at 276 nm, which should be ascribed to $\pi \rightarrow \pi^*$ transitions of aromatic amino acid residues such as tryptophan, tyrosine, and phenylalanine on protein peptide chains. The maximum absorptive intensity of the LNPs-WP dispersions was increased from the LNPs addition, suggesting that the LNPs should cause a conformation change of proteins. Remarkably, the LNPs-WP at (1:8) proportion could even cause the shielding of hydrophobic groups, resulting in decreased absorption peak intensity compared to the WP only. In addition, the morphogenesis of LNPs, WP, and LNPs-WP bioparticles was respectively observed under SEM (Fig. 1D). As a comparison, the LNPs appeared as uniform particles, but aggregation occurred between the particles accounting for a poor dispersibility of the LNPs solution. However, the WP showed a spherical folded conformation, which should effectively encapsulate hydrophobic amino acid residues within its interior while exposing hydrophilic residues to the aqueous environment, thereby achieving a good water solubility. The spherical and large-sized structures of the commercial WP observed under SEM should not present an intrinsic morphology of the native whey protein molecules, mainly due to a granulation from industrial process. During hydration under standard condition, the granulated WP particles maintain a spherical shape temporarily from the physical aggregation induced by the granulation process, consistent with the observations of previous studies (Huang et al., 2026; Zhou et al., 2026). Notably, the LNPs-WP bioparticle at (8:8) proportion formed a typical agglomeration from effective interaction between LNPs and WP, confirming a well LNPs-WP integration achieved.

3.2. Dynamic interaction of LNPs-WP bioparticles with oil-water interface

Given that the interfacial wettability of particles is vital for preparing Pickering emulsions, and that near-neutral wettability ($\theta_{ow} \approx 90^\circ$) can effectively promote particle aggregation at the oil-water interface to prevent oil droplet coalescence (Chen et al., 2022), this study modified emulsifier wettability by altering the ratio of hydrophobic LNPs to hydrophilic WP (Fig. 2). In general, the typical images of water droplets were observed by depositing on the particles immersed in soybean oil.

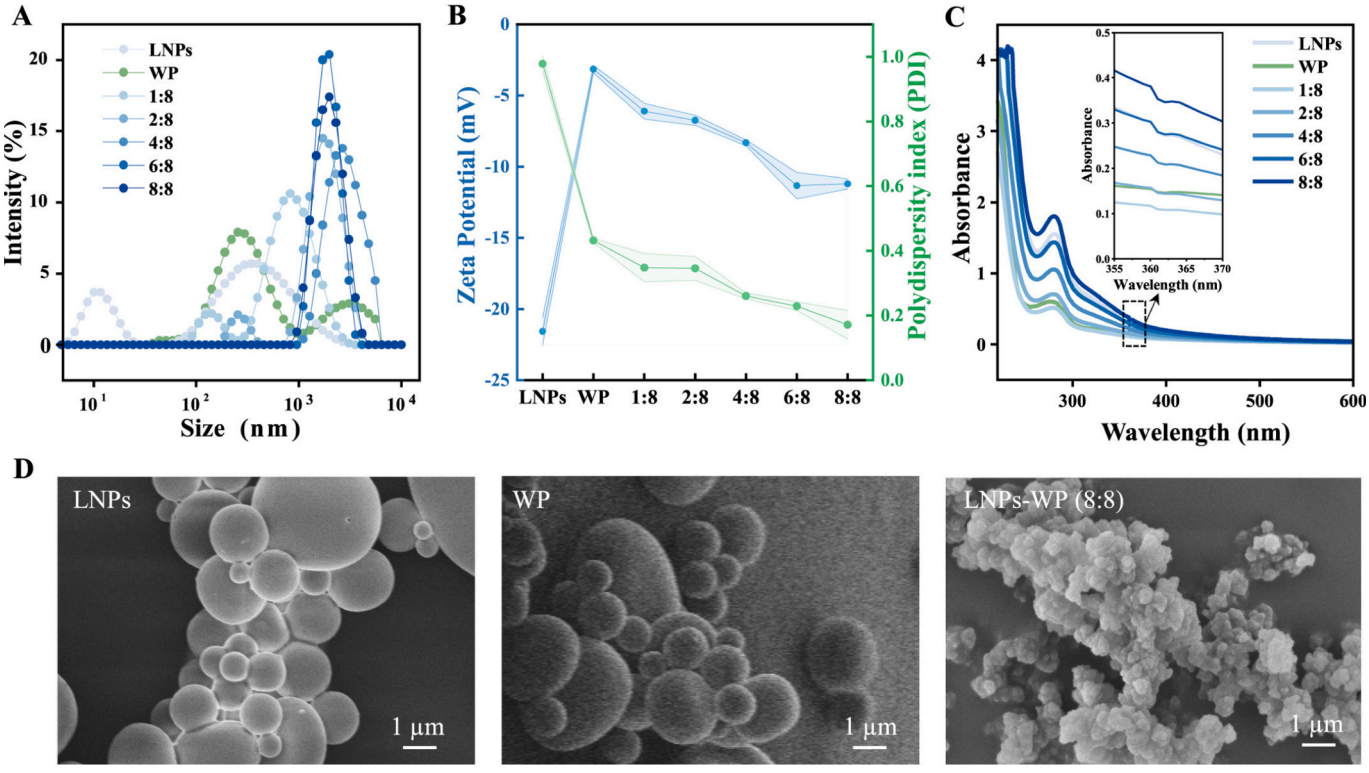

Fig. 1. Characterization of the nanocomplexes consisting of lignin nanoparticles (LNPs) and whey protein (WP) at different mass ratios (LNPs: WP). (A) Size distributions; (B) Polydispersity index and zeta potential values; (C) UV spectrum absorbances; (D) SEM images.

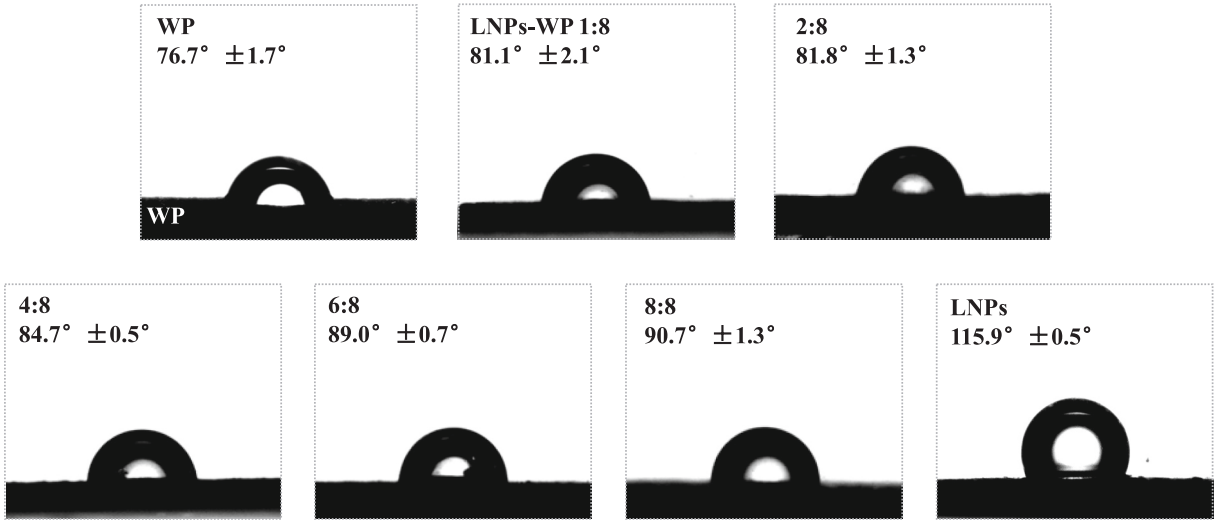

Fig. 2. Three-phase contact angles of the LNPs-WP nanocomplexes interacted at different mass ratios.

As the more LNPs were moved to the oil-water interface to participate in the formation of the interfacial film, the LNPs-WP contact angle was gradually increased. The three-phase contact angle (θ_{ow}) on the surfaces of LNPs-WP composites was then increased from 81.1° to 90.7°. In particular, the LNPs-WP samples at 6:8 and 8:8 proportions exhibited a near-neutral wetting with θ_{ow} values around 90°, indicating that the LNPs-WP bioparticles could be applied as a dynamic stabilizer for production of Pickering emulsions (Chen et al., 2021). The results thus

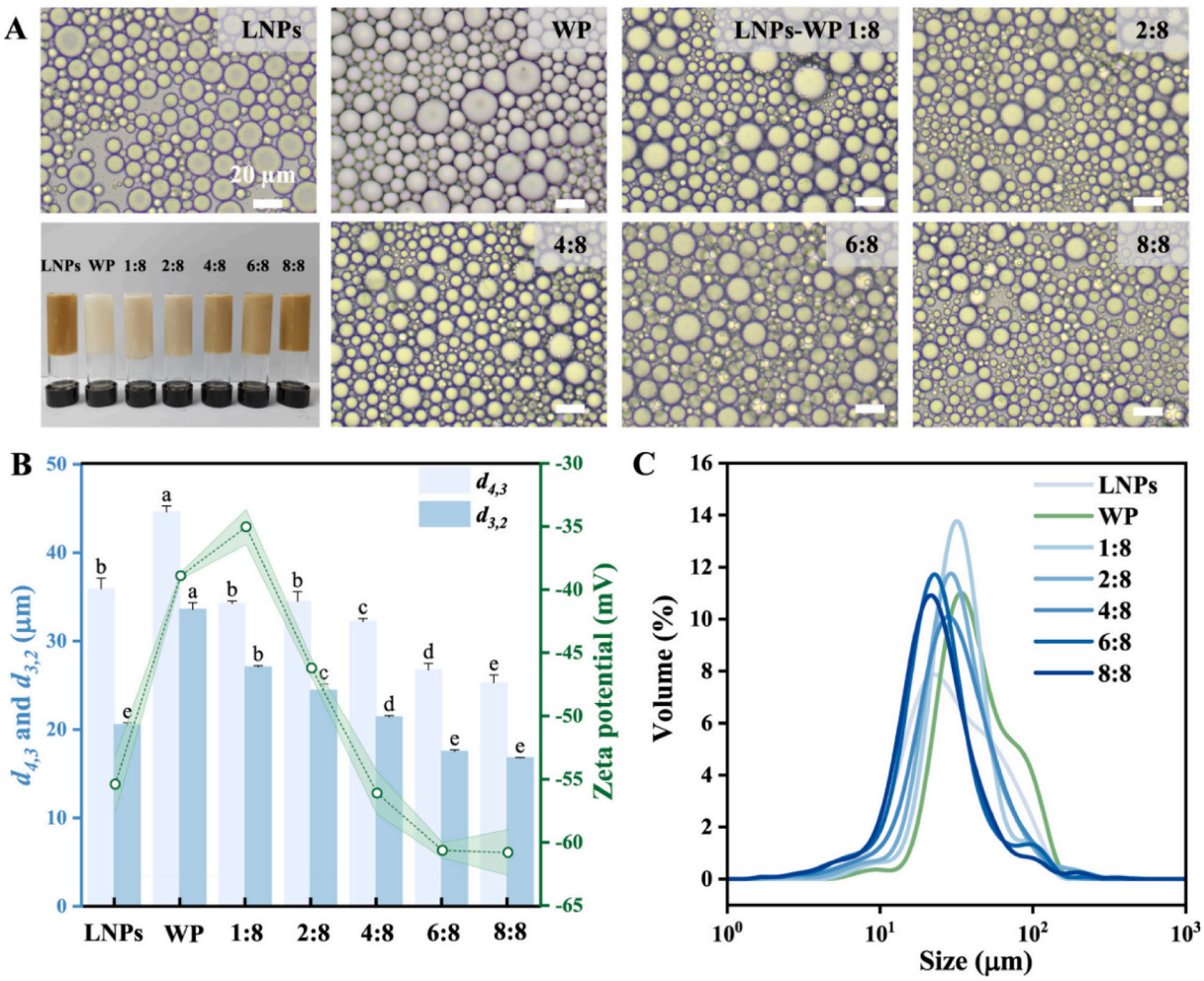

Fig. 3. Characterization of high internal phase Pickering emulsion stabilized by LNPs-WP nanocomplexes interacted at different mass ratios. (A) Optical microscope images; (B) Volume mean diameter ($d_{4,3}$), surface mean diameter ($d_{3,2}$) and zeta potential values, the letters (a-f) represent significant differences among samples; (C) Size distribution. Significant differences between samples were determined using one-way ANOVA: $p < 0.05$ ($n = 7$).

revealed that the hydrophobic LNPs and hydrophilic WP could be effectively interacted to adjust the wettability of overall particles for synergistic construction of a stable interfacial layer.

3.3. Fabrication and stability of the emulsions by LNPs-WP nanocomplexes

As a consequence, this study observed the emulsions stabilized by LNPs-WP bioparticles/nanocomplexes under optical microscopy (Fig. 3A). Among the LNPs and WP HIPPEs examined, the emulsion droplets exhibited a typical droplet flocculation and agglomeration (Fig. 3A), consistent with the results of particle size (Fig. 3B). Under the presence of high LNPs concentrations/proportions (6:8–8:8), the oil droplets were coated with adsorbed LNPs-WP particles, forming a uniform and stable emulsion gel that likely enhanced the long-term stability of the emulsion. The emulsions stabilized by low LNPs concentrations (1:8 and 2:8) exhibited larger emulsion droplets with $d_{4,3}$ of 34.29 and 34.50 μm (Fig. 3B). This phenomenon can be attributed to the fact that low-concentration LNPs lack the capacity to surmount the energy barrier associated with particle-oil interactions, thereby preventing most particles from reaching the interface (Kim et al., 2017). Moreover, the observed decrease in $d_{4,3}$ and $d_{3,2}$ as LNPs concentration increases indicated an enhancement in emulsifying ability. Moreover, the emulsions stabilized by LNPs-WP nanocomplexes showed an interesting LNPs-concentration-dependent behavior. The LNPs-WP samples had a relatively narrower droplet size distribution from high LNPs concentrations (Fig. 3C), and their $d_{4,3}$ values were smaller than those of the emulsions stabilized by low LNPs concentrations (Fig. 3B). Therefore, the formation of emulsion gels generated from LNPs-WP nanocomplexes should be mainly owning to the hydrogen bonding interactions between excess LNPs-WPs in the continuous phase and around the droplet surface, leading to a self-assembly into a three-dimensional hydrogel network.

3.4. Improved rheological properties of the emulsions stabilized by LNPs-WP

Subsequently, the deformation rheological tests comprising both oscillation and flow measurements were conducted to investigate the rheological properties of the Pickering emulsions stabilized by LNPs-WP nanocomplexes (Fig. 4). While the shear rates were increased from 0.1 s^{-1} to 100 s^{-1}, the emulsions showed a decrease in apparent viscosity and an increase in shear stress (Fig. 4A and B), which was accounting for a shear thinning behavior (Yan et al., 2022). The steady-state flows of all emulsions were diminished as the shear rates were escalated, attributable to the reduction in both intermolecular interactive forces and apparent viscosity (Zhao et al., 2023). The HIPPEs stabilized by LNPs-WP (8:8) showed remarkedly higher η values, which was ascribed to the formation of denser hydrogel network in the aqueous-phase. The emulsions stabilized by LNPs-WP exhibited a more concentrated state due to the good wettability of LNPs-WP ($\theta_{ow} = 90.7°$), forming a weak gel structure filled with particles. Meanwhile, the rigid LNPs-WP interface film inhibited oil droplet deformation with enhanced resistance to flow for a higher viscosity. The correlations among the closely packed oil droplet network, rigid interface film and elevated viscosity were consistent with the previous report (Zhang et al., 2024).

By monitoring the viscosity changes under alternating cycles of low shear rate (0.1 s^{-1}) and high shear rate (10 s^{-1}), the destruction and recovery of the HIPPEs structure were also determined (Fig. 4C). While the shear rate was increased from 0.1 s^{-1} to 10 s^{-1}, the viscosity of HIPPEs was dropped sharply, indicating that the closely packed oil droplet network and the LNPs-WP interface film structure were

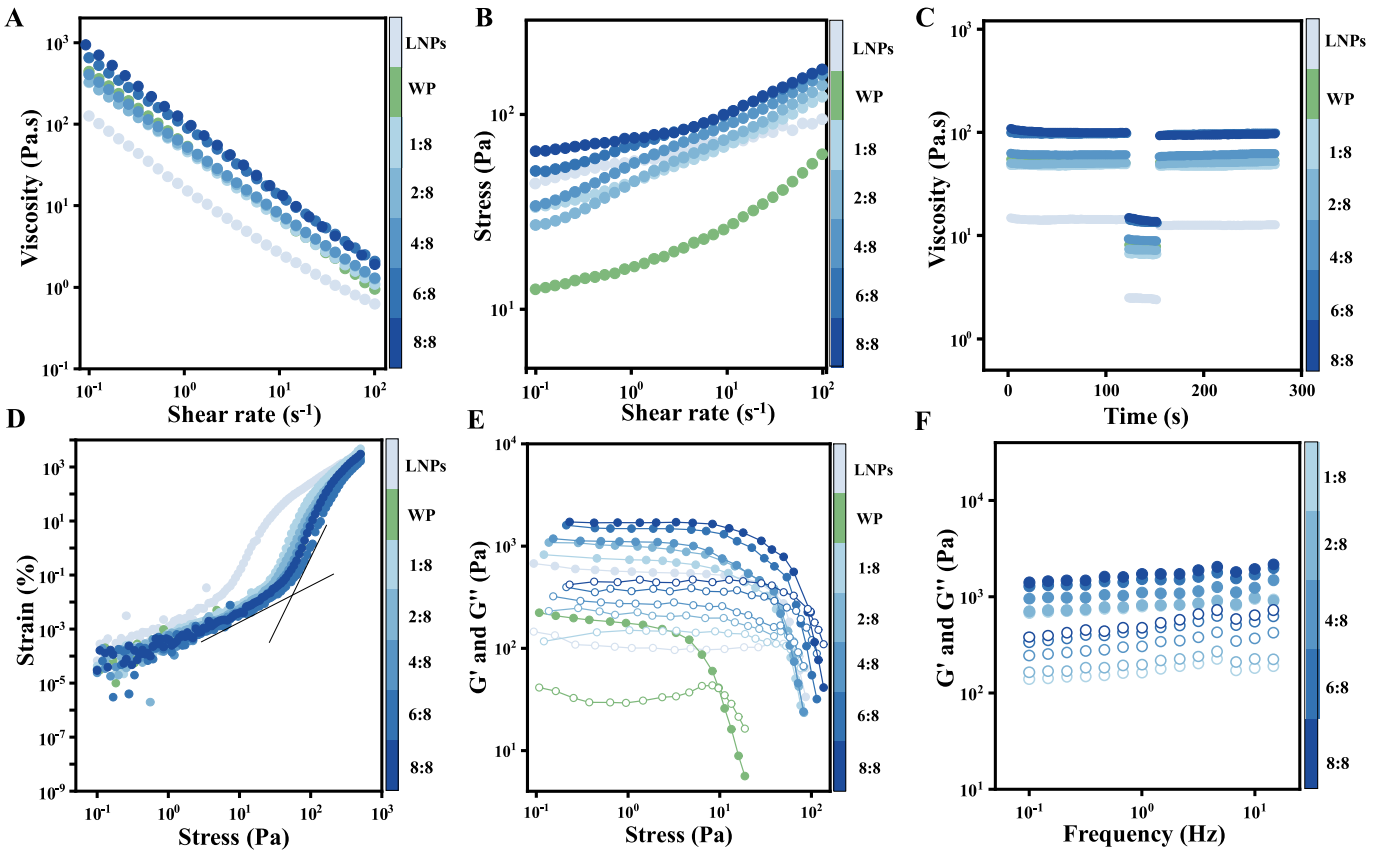

Fig. 4. The rheological properties of Pickering emulsion stabilized by LNPs-WP nanocomplexes interacted at different mass ratios. (A, B) Viscosity and stress values; (C, D) Thixotropic recovery and yield stress; (E, F) Stress sweeps and frequency sweeps. Filled and open symbols represent G′ and G″, respectively.

disrupted under high shear rates. Under the shear rate decreased from 10 s^{-1} to 0.1 s^{-1}, the viscosity of HIPPEs was immediately recovered to varying degrees, suggesting that the disrupted network structure was gradually reconstituted. This phenomenon was precisely accounting for the cause of thixotropic recovery behavior of HIPPEs. Even though the viscosity of HIPPEs was significantly varied from different LNPs concentrations, the viscosity recovery ability was gradually enhanced with increasing LNPs concentration and the emulsion with LNPs-WP (8:8) had the best recovery performance, which should be due to the strongest interaction between LNPs and WP. Such interaction not only reinforced the rigidity of the interface film but also promoted the re-formation of closely packed oil droplet network, thereby enhancing the strength of overall network structure and maximizing the resistance against instant deformation (Cheng et al., 2025).

As the minimum shear stress required to impart flowability to suspensions can be determined through yield stress measurements (Wang, Espert, Hernández, Salvador, & Sanz, 2024), this study determined the yield stress value by measuring the inflection point of the deformation and stress curve of the emulsion (Fig. 4D). In the LNPs emulsion, the yield stress was quite small (3.60 Pa), whereas the yield stress was 21.50 Pa at the WP. Despite LNPs-WP emulsions at low proportions (1:8, 2:8) remained relatively lower yield stress than that of the WP emulsion, the yield stress started to increase from high LNPs concentrations, and it reached a maximum of 31 Pa at 6:8 proportion, suggesting the maximum strength of capillary bridges. The LNPs-WP emulsion at 8:8 showing a slight decline to 30.60 Pa may be due to high oil phase content for more particles adsorbed on the surface of droplets, which decreased the distance between droplets.

The storage modulus (G') and loss modulus (G") of the emulsions were also measured as a function of stress (Fig. 4E). As G' is a metric for energy storage in the network, and its magnitude directly reflects the structural strength and elasticity of the emulsion, the higher G' values at low-stress range relative to the corresponding G" values should confirm the formation of a robust gel-like emulsion structure. The intersection points of G' and G" shifted toward higher stress values as the concentration of LNPs was increased, which indicated that the rigidness of the LNPs-WP interface film was further enhanced, the oil droplet packing became tighter, and the three-dimensional network structure was stronger with a more elastic interface. Meanwhile, the storage (G') and loss (G") moduli of the emulsions were also measured as a function of frequency (Fig. 4F). Both LNPs and WP emulsions were not detectable, but the G' and G“ values of LNPs-WP emulsions were examined with slight increase from high LNPs concentration. At low frequency (<1 Hz), G' exhibited a small slope, but both G' and G" had a weak dependence on frequency, indicating that the LNPs-WP emulsion was a stable dispersion. For emulsions stabilized by LNPs-WP at low ratios (1:8–2:8), the liquid emulsions generally had low G' values, indicating weak structural viscoelasticity due to the agglomeration of oil droplets. In contrast, samples stabilized by LNPs-WP at high ratios (4:8–8:8) exhibited high G' values, which corresponded to a stronger gel network. Taken together, the emulsion gels stabilized by LNPs-WP at high LNPs concentrations/proportions (4:8–8:8) could act as elastic and soft-textured solid-state materials from dynamic interactions of LNPs and WP at the interface and in the continuous phase, thereby leading to a stabilized Pickering emulsions achieved from effective LNPs and WP integration.

3.5. *Characteristic microstructures of HIPPEs stabilized by LNPs-WP bioparticles*

Under confocal laser scanning microscopy, this study observed the distinct microstructures of emulsions stabilized by LNPs-WP bioparticles at the oil-water interfaces by respectively staining with Nile Blue and Nile Red (Fig. 5). The emulsions samples stabilized by LNPs or WP only, showed distinct larger droplets, flocculation and aggregation, which were consistent with the particle sizes examined above (Fig. 3B). As a comparison, the emulsions samples stabilized by LNPs-WP at low proportions (1:8 and 2:8) presented a cluster of larger oil droplets, confirming a typical oil droplet flocculation. As the LNPs proportion was increased, however, the oil droplets were uniformly surrounded by the red signals, indicating that the surface of the oil droplets could be completely wrapped by the adsorbed LNPs-WP particles. Notably, the HIPPEs exhibited a similar uniform microstructure from the LNPs-WP proportion at 6:8, whereas the emulsion at 8:8 proportion developed partial droplets at less than 10 μm. This reduction in droplet size was particularly significant as it contributed to a higher interfacial area, being closely associated with enhanced encapsulation efficiency. Meanwhile, the complete wrapping of oil droplet surfaces by adsorbed LNPs-WP particles implied the formation of a thick and rigid interfacial film. Such a robust interfacial barrier could effectively prevent the leakage of encapsulated active ingredients, further boosting the

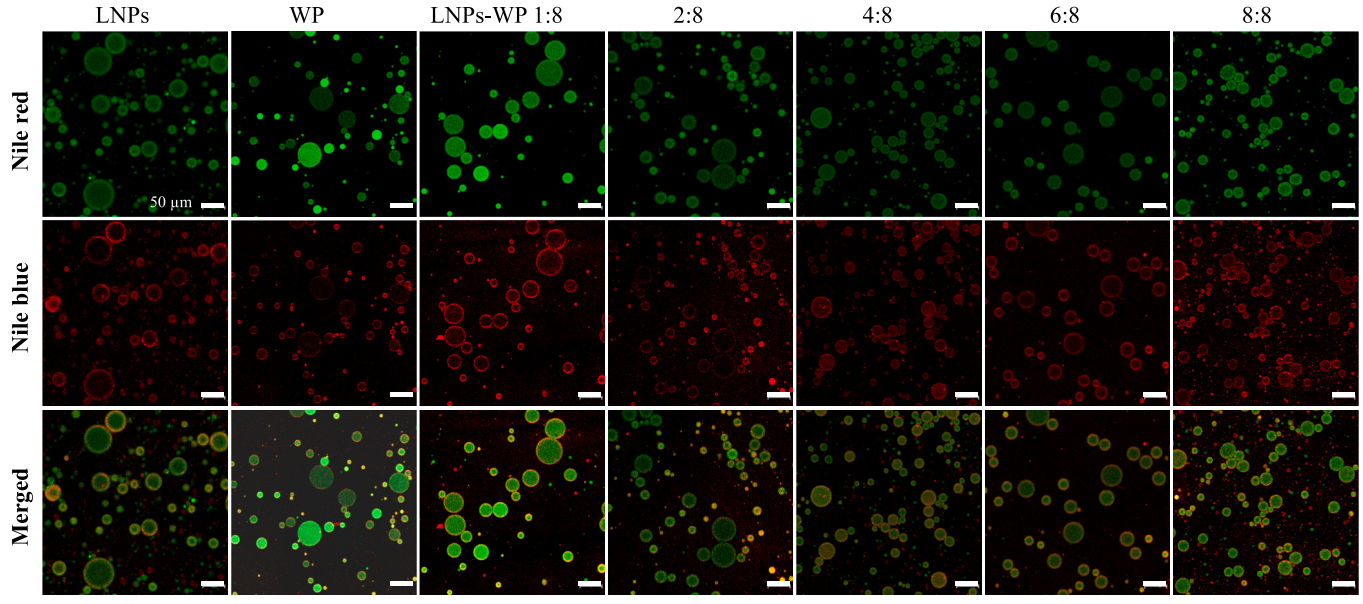

Fig. 5. Fluorescent observations of high internal phase Pickering emulsion stabilized by LNPs-WP nanocomplexes interacted at different mass ratios as CLSM images. Soybean oil stained in green and LNPs and WP nanocomplexes in red. (For interpretation of the references to colour in this figure legend, the reader is referred to the web version of this article.)

encapsulation efficiency.

Overall, the formation process of the HIPPEs microstructure was highly related to the LNPs proportion in the LNPs-WP particles. The transition toward smaller and uniformly dispersed droplets with complete interfacial coverage (as the LNPs proportion increased) not only aligned with the above reports (Figs. 2 and 3), but also provided structural basis for high encapsulation efficiency. Specifically, the high interfacial area from small droplet sizes and the protective effect of thick and rigid interfacial films could synergistically promote efficient encapsulation.

3.6. Consistently improved stability of the Pickering emulsions by LNPs-WP integration

3.6.1. Storage stability

The stability of Pickering emulsions was initially examined by calculating TSI values after storage at different incubation times (Fig. 6). By comparison, the TSI values of emulsions stabilized by individual LNPs or WP were consistently higher than those of all LNPs-WP bioparticle samples (Fig. 6A), which should be accounting for an unstable or destabilized emulsions. Among the LNPs-WP samples examined, the TSI values were decreased from relatively increased LNPs proportions, indicating that the addition of LNPs could enhance emulsion stabilization. Particularly, the LNPs-WP samples at high LNPs proportions (6:8, 8:8) had the TSI values at less than 0.2, which revealed an excellent storage stability. The optimal stability should be attributed to the three-dimensional gel network structure formed from high concentrations of LNPs by effectively restricting the movement of oil droplets and preventing their coalescence and sedimentation (Wang et al., 2022). After 90-day storage at 4 °C, all emulsions samples showed a change in particle sizes, but the optimal emulsion sample of LNPs-WP (8:8) had the least alteration (Fig. 6B), indicating an excellent stability with little destabilization during storage. The results thus demonstrated the longest storage time and the lowest TSI value in the LNPs-WP (8:8) emulsion sample.

3.6.2. Thermal stability

To further test thermal stability of three better LNPs-WP emulsions samples, this study observed their microstructures and rheological properties at 65 °C, 90 °C and 121 °C for 20 mins (Fig. 7). Fig. 7A shows that the droplets of the 4:8 emulsion coalesced after heating at 65 °C, with small droplets merging to form large droplets. Flocculation occurred at 90 °C, with the emulsion droplets agglomerating together. After heating at 121 °C, the oil droplet coalescence became more severe, and the emulsion became completely unstable, because the temperature increase can enhance the energy of molecular motion, weaken the interfacial film strength, and facilitate droplet collision and coalescence (Wang et al., 2023). After heating emulsions with high LNPs/WP ratios (6:8 and 8:8) at 65 °C for 20 mins, the oil droplet size remained unchanged. Upon heating at 90 °C, the particle size of the 6:8 emulsion increased slightly, while that of the 8:8 emulsion remained unchanged, with only slight flocculation occurring. However, the LNPs-WP (8:8) samples maintained obviously more stable than those of other two samples under three high temperatures, mainly due to the strong hydrogen bonding between LNPs (hydroxyl, carbonyl groups) and WP (amino and carboxyl groups) enabled to form a well three-dimensional network structure. This structure elevated desorption and coalescence activation energy, hindering WP-LNPs desorption from the interface and oil droplet fusion (Binks & Horozov, 2007). As high temperature has a critical impact on emulsion viscosity (Chevallier et al., 2016), this study also detected viscosity alteration among three LNPs-WP emulsions samples (Fig. 7B-E). As the temperature increased, the viscosity of the emulsion gradually increased. This was because the temperature increase may cause the conformation of the polymer chains to change, such as from a tightly coiled state to a more extended state, which increased the viscosity (Zhang, Zhang, Zhong, Qi, & Li, 2022). The above results showed that the optimal LNPs-WP (8:8) emulsion can still maintain a stable microstructure and good rheological properties when heated at 90 °C.

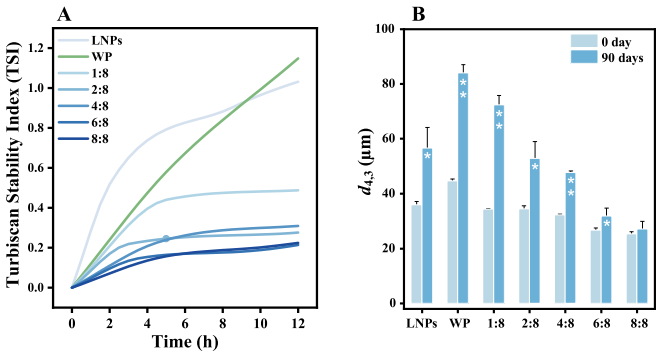

Fig. 6. Pickering emulsion stability among LNPs-WP nanocomplexes and individual LNPs or WP sample. (A) Turbiscan Stability Index (TSI) under different incubation times; (B) Volume average size ($d_{4,3}$) values after 90 days storage. Significant differences between the 0 day and 90 days were determined using two-tailed Student's *t*-test: $^{**}p < 0.01$, $^{*}p < 0.05$ ($n = 2$).

3.6.3. Oil volume fraction impact

For two desired LNPs-WP (6:8, 8:8) samples, this study detected their oil phase fractions (85%–90%) impacts on emulsion stability (Fig. 8). In general, the microstructure of dispersed phase was altered from increasing ø, and in particular under the ø value at 85%, the emulsions exhibited uniform and spherical droplets with relatively evenly dispersed in the continuous aqueous phase (Fig. 8A). Under the ø value at 88% or 90%, raised dispersed phase concentrations only led to a slight increase in the volume of dispersed droplets, indicating that coarser emulsions were constructed at higher ø values. However, the LNPs-WP (8:8) emulsion sample exhibited relatively smaller particle sizes than the emulsion (6:8) did (Fig. 8B), confirming that the LNPs-WP (8:8) integration should be optimal for preparing ultra-high internal phase emulsions with a dispersed phase volume fraction of 90%.

3.6.4. Ion concentration impact

Since the ionic concentration is another important factor on emulsion stability (Zhao et al., 2025), this study employed different concentrations of NaCl (0–1000 mM) to test their impacts on the optimal LNPs-WP (8:8) sample (Fig. 9). While NaCl concentration was raising, the emulsion droplet size was relatedly increased with slight aggregation (Fig. 9A), mainly due to the electrostatic shielding effect at high ionic strength (Mi, Xia, Zhang, Liu, & Cai, 2022). Meanwhile, the viscosity analyses showed that the optimal emulsions sample was of a strong shear-thinning property (Fig. 9B), suggesting that different concentrations of NaCl could improve the viscosity of the LNPs-WP emulsions at high shear rates, consistent with the previous report (He et al., 2023). Furthermore, this study determined NaCl impact on viscoelastic properties, and the G' values were much higher than those of G" across entire frequency range (Fig. 9C), indicating that the optimal LNPs-WP (8:8) emulsions could well behave from an elastic three-dimensional network. At low frequencies (≤1 Hz), the G' showed a smaller slope to account for stable emulsions from ions addition. We thus assumed that the LNPs-WP complexes should construct other stabilization mechanisms that counteracted the destabilizing effect of ionic electrostatic screening on emulsion stability. After the LNPs as a rigid aromatic ring structure bind to whey protein through mechanisms including hydrophobic interactions, hydrogen bonding, and covalent cross-linking, a dense and thick interfacial film is thus formed. In this case, the emulsion stabilization mechanism may be dominated by steric hindrance effects. Even while ions screen the charges, the physical barrier of the interfacial film can still prevent droplet aggregation and coalescence to maintain

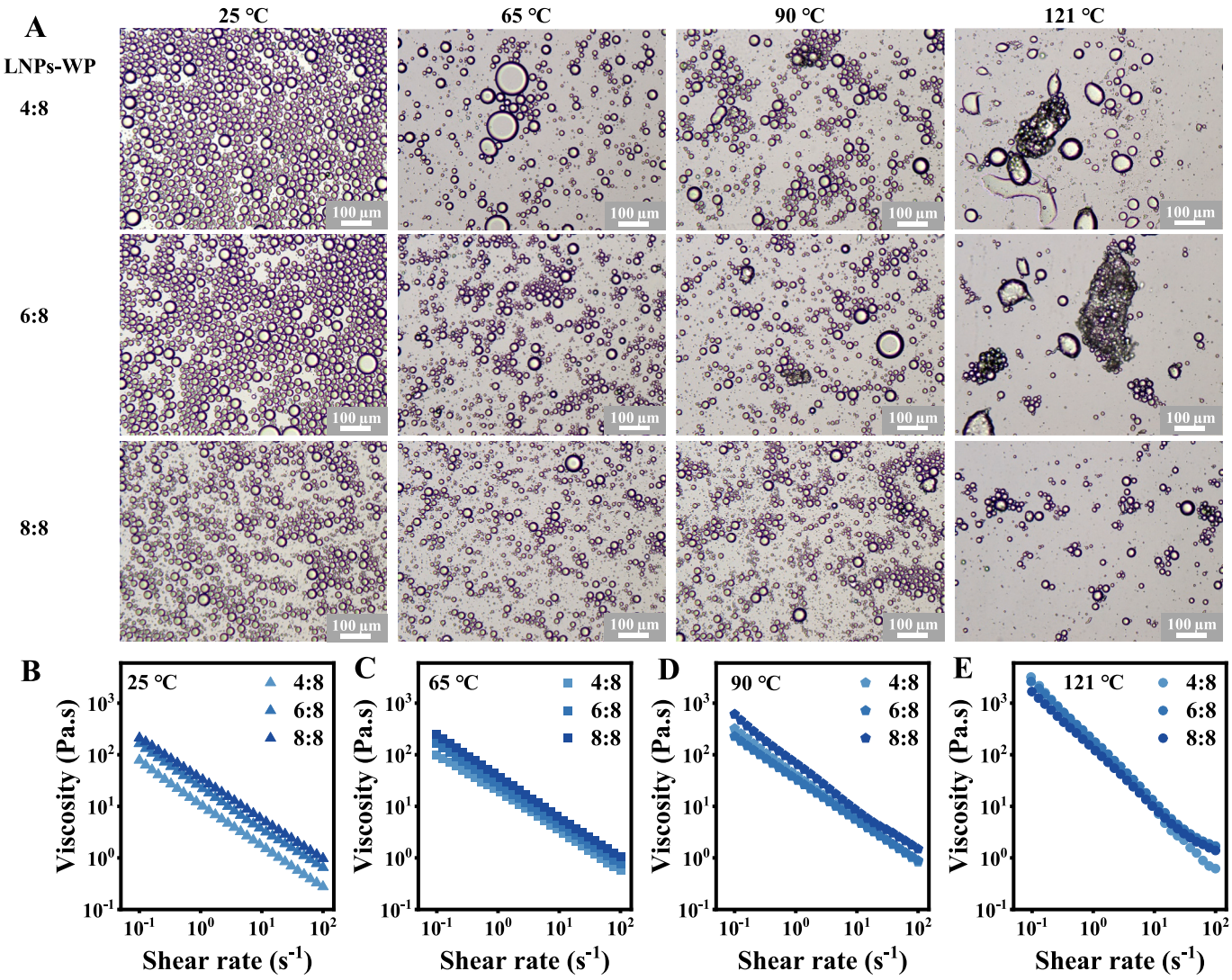

Fig. 7. The thermal stability of Pickering emulsion among three LNPs-WP nanocomplexes samples under high temperatures for 20 min. (A) Microscopic images; (B—D) Viscosity variations.

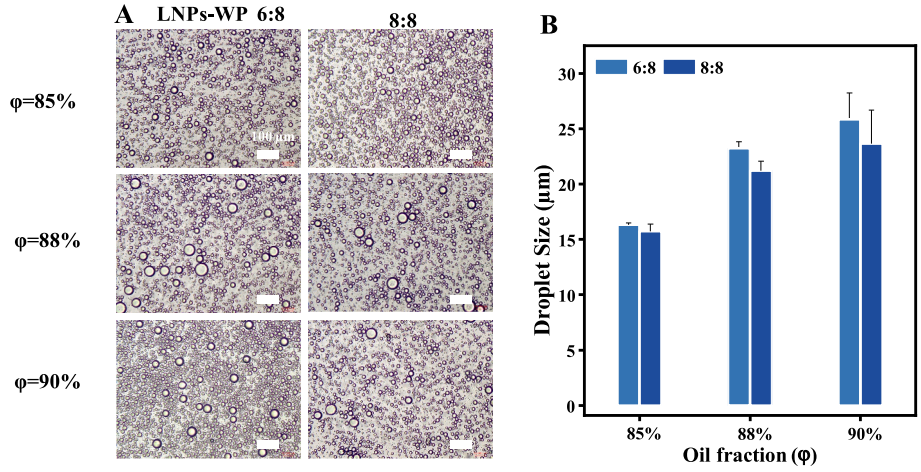

Fig. 8. The stability of Pickering emulsion with different oil-volume fractions among two LNPs-WP nanocomplexes samples. (A) Optical microscope images; (B) Droplet sizes.

emulsion stability. Therefore, the introduction of LNPs could significantly enhance the mechanical strength and toughness of the interfacial film, and the rigid structure of LNPs could fill the gaps between whey protein molecules to reduce defects in the interfacial film. Meanwhile,

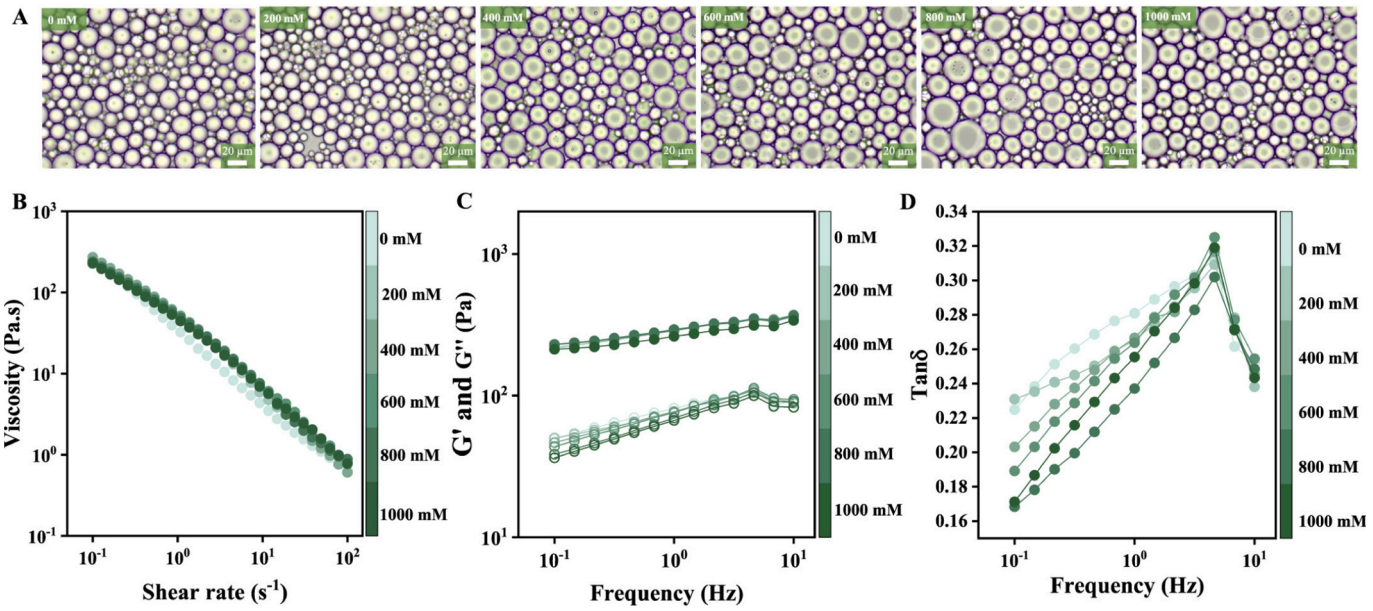

Fig. 9. Characterization of Pickering emulsion stabilized by optimal LNPs-WP (8:8) under different ionic strengths (0–1000 mM). (A) Microscopic images; (B) Viscosity variations; (C) Frequency sweeps; (D) Loss tangents. Filled and open symbols represent G′ and G″, respectively.

the multiple interactions between LNPs and WP enabled the formation of a network structure within the emulsion, substantially improving its resistance to external disturbances. In addition, this study examined all emulsion samples with tanδ values at less than 1.0 (Fig. 9D), and a low tanδ should confirm the predominantly elastic (solid-like) nature of the HIPPE network for long-term physical stability and potential application as a delivery vehicle. As the ion concentration was increased (0–800 mM), the tanδ values were gradually decreased from 0.225 to 0.168, confirming that the addition of salt ions could greatly improve emulsion ability to resist external interference. However, while the salt ion concentration was further increased to 1000 mM, the tanδ value was slightly increased, suggesting that extremely high ions concentration should destroy network structure of emulsions and cause the elastic solid to transform into a viscous fluid. In conclusion, the optimal LNPs-WP (8:8) emulsion sample was of great stability for salt ions stress under high concentrations.

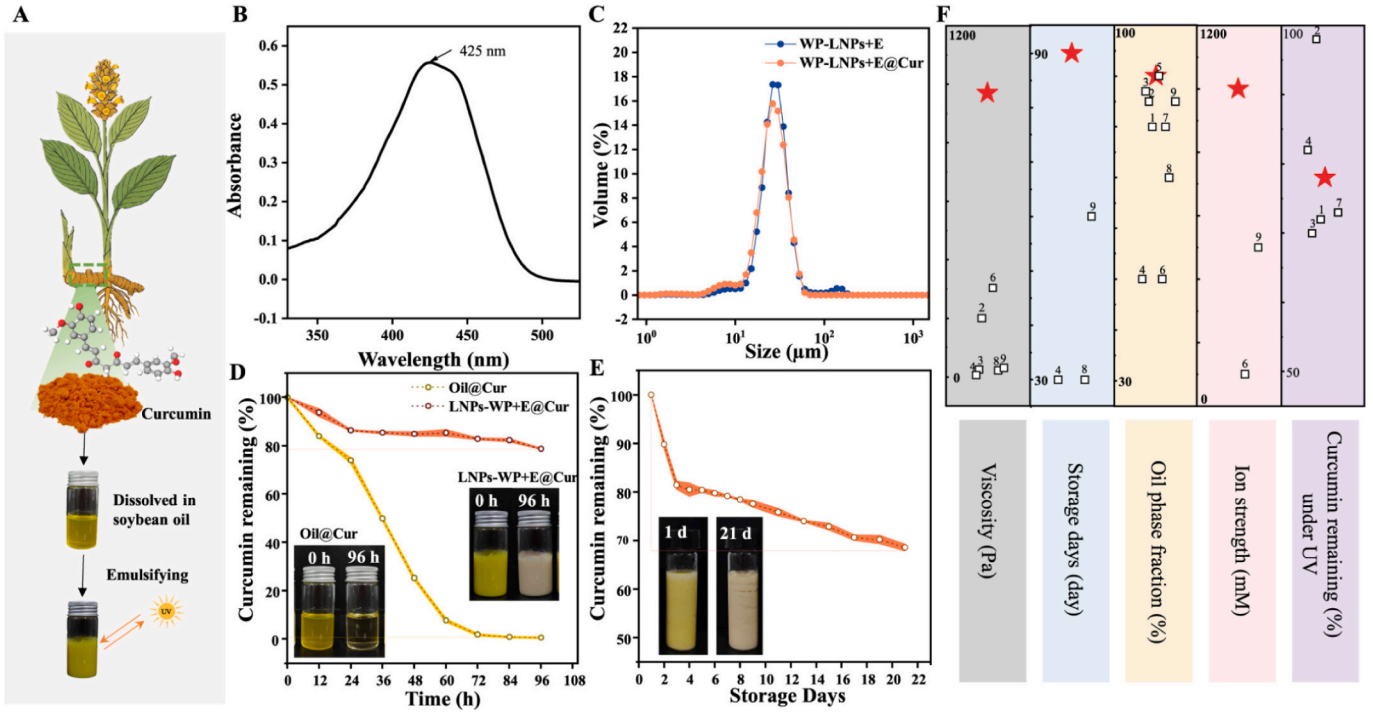

Fig. 10. The multiple-properties-improved model of curcumin-encapsulated emulsions stabilized by the optimal LNPs-WP (8:8) nanocomplexes. (A) Schematic diagram of curcumin encapsulated in the emulsion stabilized by LNPs-WP; (B) Visible light absorption spectrum of curcumin; (C) Psize distribution; (D) UV irradiation stability; (E) Storage stability; (F) Comparison of Pickering emulsions with the previously-reported ones using other lignin substrates as stabilizers as shown in Table S1.

3.7. The property-improved model of curcumin-encapsulated emulsion

By dissolving the curcumin with soybean oil, this study prepared an emulsion with a curcumin concentration of 0.185 mg/mL (Fig. 10A). The curcumin content in emulsion was determined by UV spectrophotometry with retention rate calculated (Fig. 10B). As a result, the particle sizes in the emulsion were not much altered before and after curcumin encapsulation (Fig. 10C), indicating that the stability of emulsion was not affected by curcumin. As curcumin was easily degraded under UV light (Bertolo et al., 2019), this study detected the change of curcumin retention rate (Fig. 10D). After irradiation at 30 W for 96 h, the curcumin retention rate remained 78% in the LNPs-WP emulsion sample, whereas the control rate (curcumin only) was reduced to 0.64%, revealing that the interface layer formed by optimal LNPs-WP sample could absorb partial UV light for reducing photooxidative damage. It was also assumed that the three-dimensional gel network structure should hinder the movement of curcumin molecules for reducing its degradation rate (Chen et al., 2020). Notably, after 21-day storage, the curcumin retention rate at 69% remained in the emulsion accountable for a storage stability (Fig. 10E), which should be due to the three-dimensional network structure formed by LNPs-WP effective for encapsulating curcumin in the oil phase and reducing its migration to water phase (Zhang et al., 2023). Finally, this study performed a broad comparison between the optimal LNPs-WP emulsion sample and the previously-reported ones stabilized by other natural emulsifiers (Fig. 10F; Table S1). Except the UV resistance, the optimal LNPs-WP emulsion showed four more excellent properties than the previously-reported ones, revealing that the LNPs-WP composite system has great applications in the encapsulation and protection of functional ingredients.

4. Conclusion

By optimizing lignin nanoparticles (LNPs) integration with whey protein (WP), this study comprehensively improved Pickering emulsions properties by the LNPs-WP nanocomplexes. The optimal LNPs-WP at high proportion (8:8) was of effective interaction for appropriate nanocomplexes assembly by electrostatic attraction with a three-phase contact angle approaching 90°, which allowed them anchoring at the oil/water interface to form a stable interfacial film that remarkably improved emulsion stability. Notably, the LNPs changed the rheological properties of WP-stabilized emulsions, and reduced creaming and coalescence by forming tightly packed, non-deformable oil droplets and the rigid LNPs-WP interfacial film, thereby increasing the electrostatic repulsion and steric hindrance between droplets for ultimately improved emulsions stability. Furthermore, the optimal LNPs-WP emulsion sample exhibited superior properties such as storage stability over 90 days, thermal stability up to 90 °C, ionic resistance up to 1000 mM NaCl, and superior UV protection, which were mostly better than the previously-reported ones stabilized by other lignin-based emulsion. Hence, this study has demonstrated a novel strategy for production of multiple-improved emulsions using natural LNPs and WP, providing insights into broad emulsion applications such as the HIPPEs for either high-temperature sterilization of high-oil functional foods or high-electrolyte formulations like antiperspirants and sea salt skincare products or for long-term storage and sterilization processes of pharmaceutical preparations.

CRediT authorship contribution statement

Guilan Zhao: Writing – original draft, Methodology, Investigation, Formal analysis. **Qian Zhang:** Writing – original draft, Investigation, Formal analysis. **Yongtai Wang:** Validation, Methodology, Formal analysis. **Xiaojie Gao:** Writing – review & editing, Methodology. **Fei Huang:** Methodology, Formal analysis. **Jiale Liu:** Methodology, Formal analysis. **Hao Peng:** Visualization, Methodology, Investigation. **Chunxiang Fu:** Supervision, Methodology. **Yanting Wang:** Writing – review & editing, Supervision, Funding acquisition. **Liangcai Peng:** Writing – review & editing, Supervision, Funding acquisition, Conceptualization.

Declaration of competing interest

The authors declare that they have no known competing financial interests or personal relationships that could have appeared to influence the work reported in this paper.

Acknowledgements

This work was in part supported by the National Natural Science Foundation of China (32470273, 32570317, 32170268, 32101701), Hubei Provincial Natural Science Foundation of China for Excellent Young Scientists (2024AFA100), the National 111 Project of the Ministry of Education of China (D17009), and the Initiative Grant of Hubei University of Technology for High-level Talents (GCC20230001).

Appendix A. Supplementary data

Supplementary data to this article can be found online at https://doi.org/10.1016/j.foodchem.2026.148452.

Data availability

Data will be made available on request.

References

Bai, L., Greca, L. G., Xiang, W., Lehtonen, J., Huan, S., Nugroho, R. W. N., … Rojas, O. J. (2019). Adsorption and assembly of cellulosic and lignin colloids at oil/water interfaces. *Langmuir, 35*(3), 571–588. https://doi.org/10.1021/acs.langmuir.8b01288

Bertolo, M. R., de Paiva, L. B. B., Nascimento, V. M., Gandin, C. A., Neto, M. O., Driemeier, C. E., & Rabelo, S. C. (2019). Lignins from sugarcane bagasse: Renewable source of nanoparticles as Pickering emulsions stabilizers for bioactive compounds encapsulation. *Industrial Crops and Products, 140*, Article 111591. https://doi.org/10.1016/j.indcrop.2019.111591

Binks, B. P., & Horozov, T. S. (2007). Colloidal particles at liquid interfaces. *Physical Chemistry Chemical Physics, 9*(48), 6298–6299. https://doi.org/10.1039/B716587K

Burgos-Díaz, C., Garrido-Miranda, K. A., Palacio, D. A., Chacón-Fuentes, M., Opazo-Navarrete, M., & Bustamante, M. (2023). Food-grade oil-in-water (O/W) Pickering emulsions stabilized by Agri-food byproduct particles. *Colloids Interfaces, 7*(2), 27. https://doi.org/10.3390/colloids7020027

Calabrese, V., Courtenay, J. C., Edler, K. J., & Scott, J. L. (2018). Pickering emulsions stabilized by naturally derived or biodegradable particles. *Current Opinion in Green and Sustainable Chemistry, 12*, 83–90. https://doi.org/10.1016/j.cogsc.2018.07.002

Chen, K., Lei, L., Lou, H., Niu, J., Yang, D., Qiu, X., & Qian, Y. (2020). High internal phase emulsions stabilized with carboxymethylated lignin for encapsulation and protection of environmental sensitive natural extract. *International Journal of Biological Macromolecules, 158*, 430–442. https://doi.org/10.1016/j.ijbiomac.2020.04.106

Chen, K., Qian, Y., Wang, C., Yang, D., Qiu, X., & Binks, B. P. (2021). Tumor microenvironment-responsive, high internal phase Pickering emulsions stabilized by lignin/chitosan oligosaccharide particles for synergistic cancer therapy. *Journal of Colloid and Interface Science, 591*, 352–362. https://doi.org/10.1016/j.jcis.2021.02.012

Chen, Y., Yi, X., Zhang, Z., Ding, B., Li, Z., & Luo, Y. (2022). High internal phase Pickering emulsions stabilized by tannic acid-ovalbumin complexes: Interfacial property and stability. *Food Hydrocolloids, 125*, Article 107332. https://doi.org/10.1016/j.foodhyd.2021.107332

Cheng, Y., Dai, Q., Lv, J., Wang, Y., Sun, T., Li, Z., Liu, Y., Huan, S., Liu, S., & Bai, L. (2025). Pickering food emulsions stabilized by bio-nanopcomplexes: Super high internal phase and 3D printability. *Food Hydrocolloids, 165*, Article 111251. https://doi.org/10.1016/j.foodhyd.2025.111251

Chevallier, M., Riaublanc, A., Lopez, C., Hamon, P., Rousseau, F., & Croguennec, T. (2016). Aggregated whey proteins and trace of caseins synergistically improve the heat stability of whey protein-rich emulsions. *Food Hydrocolloids, 61*, 487–495. https://doi.org/10.1016/j.foodhyd.2016.06.009

Davtalab, M., Naji-Tabasi, S., Shahidi-Noghabi, M., Martins, A. J., Bourbon, A. I., & Cerqueira, M. A. (2024). Pickering emulsion stabilized by different concentrations of whey protein–cress seed gum nanoparticles. *Foods, 13*(23), Article 3777. https://doi.org/10.3390/foods13233777

Gan, J., Zhan, Y., Fan, J., Wang, J., Gao, Q., Huang, C., Yu, W., & Zhang, K. (2025). Pickering multiphase materials using plant-based colloidal lignin nanoparticles. *Green Chemistry, 27*(5). https://doi.org/10.1039/D4GC05713A

He, X., Wang, B., Xue, Y., Li, Y., Hu, M., He, X., Chen, J., & Meng, Y. (2023). Effects of high acyl gellan gum on the rheological properties, stability, and salt ion stress of sodium caseinate emulsion. *International Journal of Biological Macromolecules, 234*, Article 123675. https://doi.org/10.1016/j.ijbiomac.2023.123675

Hellwig, M., Humpf, H.-U., Hengstler, J., Mally, A., Vieths, S., & Henle, T. (2019). Quality criteria for studies on dietary glycation compounds and human health: Opinion of the senate commission on food safety (SKLM) of the German research foundation (DFG). *Journal of Agricultural and Food Chemistry, 67*(41), 11307–11311. https://doi.org/10.1021/acs.jafc.9b04172

Huang, Z., Pang, L., Li, R., Shi, J., Zhao, Q., Jiang, Y., Yang, X., & Qu, B. (2026). Study on the effect of glycosylation reaction in wet mixing on the emulsifying properties of extensively whey protein hydrolysates. *Food Chemistry, 503*, Article 147764. https://doi.org/10.1016/j.foodchem.2025.147764

Jiang, H., Sheng, Y., & Ngai, T. (2020). Pickering emulsions: Versatility of colloidal particles and recent applications. *Current Opinion in Colloid & Interface Science, 49*, 1–15. https://doi.org/10.1016/j.cocis.2020.04.010

Kim, K., Kim, S., Ryu, J., Jeon, J., Jang, S. G., Kim, H., … Kim, H. (2017). Processable high internal phase Pickering emulsions using depletion attraction. *Nature. Communications, 8*(1), 14305. https://doi.org/10.1038/ncomms14305

Li, R., Guo, Y., Dong, A., & Yang, X. (2023). Protein-based emulsion gels as materials for delivery of bioactive substances: Formation, structures, applications and challenges. *Food Hydrocolloids, 144*, Article 108921. https://doi.org/10.1016/j.foodhyd.2023.108921

Li, X., Fan, L., & Li, J. (2023). Extrusion-based 3D printing of high internal phase emulsions stabilized by co-assembled β-cyclodextrin and chitosan. *Food Hydrocolloids, 134*, Article 108036. https://doi.org/10.1016/j.foodhyd.2022.108036

Li, Y., He, B., Zhang, H., Liu, J., Li, S., Kang, H., et al. (2024). Enriched extensin and cellulose for non-collapse biochar assembly to maximize carbon porosity and dye adsorption with high bioethanol production. *Industrial Crops and Products, 222*, Article 119924. https://doi.org/10.1016/j.indcrop.2024.119924

Li, Y., Yang, D., Wang, S., Xu, H., & Li, P. (2024). Fabrication and optimization of Pickering emulsion stabilized by lignin nanoparticles for curcumin encapsulation. *ACS Omega, 9*(20), 21994–22002. https://doi.org/10.1021/acsomega.3c10395

Mi, S., Xia, M., Zhang, X., Liu, J., & Cai, Z. (2022). Formation of natural egg yolk granule stabilized Pickering high internal phase emulsions by means of NaCl ionic strength and pH change. *Foods, 11*, 229. doi:10.3390/ foods11020229.

Mikkonen, K. S. (2020). Strategies for structuring diverse emulsion systems by using wood lignocellulose-derived stabilizers. *Green Chemistry, 22*(4), 1019–1037. https://doi.org/10.1039/C9GC04457D

Moreno, A., & Sipponen, M. H. (2020). Biocatalytic nanoparticles for the stabilization of degassed single electron transfer-living radical Pickering emulsion polymerizations. *Nature Communications, 11*(1), Article 5599. https://doi.org/10.1038/s41467-020-19407-3

Naji-Tabasi, S., Mahdian, E., Arianfar, A., & Naji-Tabasi, S. (2021). Nanoparticles fabrication of soy protein isolates and basil seed gum (*Ocimum bacilicu* L.) complex as Pickering stabilizers in emulsions. *Journal of Dispersion Science and Technology, 42*(5), 633–640. https://doi.org/10.1080/01932691.2019.1703736

Peng, H., Zhao, W., Liu, J., Liu, P., Yu, H., Deng, J., Yang, Q., Zhang, R., Hu, Z., Liu, S., Sun, D., Peng, L., & Wang, Y. (2022). Distinct cellulose nanofibrils generated for improved Pickering emulsions and lignocellulose-degradation enzyme secretion coupled with high bioethanol production in natural rice mutants. *Green Chemistry, 24*(7), 2975–2987. https://doi.org/10.1039/D1GC04447H

Qin, K., Sun, X., Liu, J., Wang, R., Huang, X., Wang, Y., Wang, H., Yang, J., & Wang, S. (2025). A rosmarinic acid-fish skin protein-chitosan hybrid nano-delivery system with excellent sustained-release and antioxidant performances. *Food Chemistry, 491*, Article 145316. https://doi.org/10.1016/j.foodchem.2025.145316

Sarabandi, K., Tamjidi, F., Akbarbaglu, Z., Samborska, K., Gharehbeglou, P., Kharazmi, M. S., & Jafari, S. M. (2022). Modification of whey proteins by sonication and hydrolysis for the emulsification and spray drying encapsulation of grape seed oil. *Pharmaceutics, 14*(11), 2434. https://doi.org/10.3390/pharmaceutics14112434

Shomali, Z., & Fatehi, P. (2022). Carboxyalkylated lignin nanoparticles with enhanced functionality for oil-water Pickering emulsion systems. *ACS Sustainable Chemistry & Engineering, 10*(50), 16563–16577. https://doi.org/10.1021/acssuschemeng.2c04143

Tao, J., Zhu, L., Zhu, L., Lei, L., & Zhao, G. (2024). Colloidal lignin preinforces the stability of Pickering emulsions prepared with zein nanoparticle. *Food Chemistry, 460*, Article 140581. https://doi.org/10.1016/j.foodchem.2024.140581

Wan, X., Kang, Q., Li, J., Guo, M., Li, P., Shi, H., Zhang, X., Liu, Z., & Xia, G. (2024). Effect of NaCl concentration on the formation of high internal phase emulsion based on whey protein isolate microgel particles. *Food Chemistry, 433*, Article 137395. https://doi.org/10.1016/j.foodchem.2023.137395

Wang, M., Wang, Y., Liu, J., Yu, H., Liu, P., Yang, Y., Sun, D., Kang, H., Wang, Y., Tang, J., Fu, C., & Peng, L. (2024). Integration of advanced biotechnology for green carbon. *Green Carbon, 2*(2), 164–175. https://doi.org/10.1016/j.greenca.2024.02.006

Wang, N., Wang, D., Xing, K., Han, X., Gao, S., Wang, T., Yu, D., & Elfalleh, W. (2023). Ultrasonic treatment of rice bran protein-tannic acid stabilized oil-in-water emulsions: Focus on microstructure, rheological properties and emulsion stability. *Ultrasonics Sonochemistry, 99*, Article 106577. https://doi.org/10.1016/j.ultsonch.2023.106577

Wang, Q., Espert, M., Hernández, M. J., Salvador, A., & Sanz, T. (2024). Effect of cellulose ether emulsion and oleogel as healthy fat alternatives in cream cheese. Linear and nonlinear rheology, texture and sensory properties. *Food Hydrocolloids, 150*, Article 109740. https://doi.org/10.1016/j.foodhyd.2024.109740

Wang, S., Zhao, H., Qu, D., Yang, L., Zhu, L., Song, H., & Liu, H. (2022). Destruction of hydrogen bonding and electrostatic interaction in soy hull polysaccharide: Effect on emulsion stability. *Food Hydrocolloids, 124*, Article 107304. https://doi.org/10.1016/j.foodhyd.2021.107304

Yan, S., Xu, J., Liu, G., Du, X., Hu, M., Zhang, S., Jiang, L., Zhu, H., Qi, B., & Li, Y. (2022). Emulsions co-stabilized by soy protein nanoparticles and tea saponin: Physical stability, rheological properties, oxidative stability, and lipid digestion. *Food Chemistry, 387*, Article 132891. https://doi.org/10.1016/j.foodchem.2022.132891

Yu, H., Zhang, G., Liu, J., Liu, P., Peng, H., Teng, Z., Li, Y., Ren, X., Fu, C., Tang, J., Li, M., Wang, Y., Wang, L., & Peng, L. (2025). A functional cascading of lignin modification via repression of caffeic acid O-methyltransferase for bioproduction and anti-oxidation in rice. *Journal of Advanced Research*. https://doi.org/10.1016/j.jare.2025.01.048

Zhang, D., Yang, Y., Li, R., Rong, X., Zhang, W., Zhang, M., Li, B., & Zhang, X. (2024). Effects of co-assembly of gliadin and carboxymethyl cellulose on the high internal phase Pickering emulsions: Rheology properties, 3D printing performance and oil-soluble nutrient delivery. *Food Hydrocolloids, 155*, Article 110162. https://doi.org/10.1016/j.foodhyd.2024.110162

Zhang, G., Wang, L., Li, X., Bai, S., Xue, Y., Peng, L., et al. (2020). Distinctively altered lignin biosynthesis by site-modification of *OsCAD2* for enhanced biomass saccharification in rice. *GCB Bioenergy, 13*, 305–319. https://doi.org/10.1111/gcbb.12772

Zhang, H., Yue, F., Hu, S., Qi, H., & Lu, F. (2023). Nanolignin-based high internal phase emulsions for efficient protection of curcumin against UV degradation. *International Journal of Biological Macromolecules, 228*, 178–185. https://doi.org/10.1016/j.ijbiomac.2022.12.123

Zhang, X., Zhang, S., Zhong, M., Qi, B., & Li, Y. (2022). Soy and whey protein isolate mixture/calcium chloride thermally induced emulsion gels: Rheological properties and digestive characteristics. *Food Chemistry, 380*, Article 132212. https://doi.org/10.1016/j.foodchem.2022.132212

Zhao, G., Wang, S., Li, Y., Liu, X., Yang, L., Song, H., & Liu, H. (2024). Metal cation-induced conformational changes of soybean protein isolate/soybean soluble polysaccharide and their effects on high-internal-phase emulsion properties. *Journal of the Science of Food and Agriculture, 104*(6), 3341–3351. https://doi.org/10.1002/jsfa.13219

Zhao, G., Wang, S., Li, Y., Yang, L., & Song, H. (2023). Properties and microstructure of Pickering emulsion synergistically stabilized by silica particles and soy hull polysaccharides. *Food Hydrocolloids, 134*, Article 108084. https://doi.org/10.1016/j.foodhyd.2022.108084

Zhao, G., Wang, S., Yang, L., Wang, P., Han, L., & Liu, H. (2025). Stability of electrostatically stabilized Pickering emulsion of silica particles and soy hull polysaccharides: Mechanism of pH and ionic strength. *Food Chemistry, 471*, Article 142804. https://doi.org/10.1016/j.foodchem.2025.142804

Zhou, X., Liu, E., Li, J., Chen, F. F., Zhang, Y., Chen, K., & Qi, D. (2023). Facile synthesis of rodlike TiO_2/lignin nanostructures as multifunctional emulsifiers for high internal phase emulsions. *ACS Applied Nano Materials, 6*, 14820–14830. https://doi.org/10.1021/acsanm.3c02384

Zhou, Z., Jiang, H., He, J., Wang, C., Xu, Y., Hou, Z., Chen, J., & Liu, X. (2026). Direct oil structuring using engineered whey protein particles: Rheological characterization and application in chocolate formulation. *Food Research International, 223*(2), 117878. https://doi.org/10.1016/j.foodres.2025.117878

Zhu, F. (2024). Modifications of whey proteins for emulsion based applications: Current status, issues and prospectives. *Food Research International, 178*, Article 113935. https://doi.org/10.1016/j.foodres.2024.113935